SINTEK JURNAL: Jurnal Ilmiah Teknik Mesin
p-ISSN: 2088-9038, e-ISSN: 2549-9645

https://jurnal.umj.ac.id/index.php/sintek

Material Selection for Fatigue Resistance in Coal Screening Systems: Finite Element Analysis of HB400 and GS20Mn5 at PT Bukit Asam Tarahan Port

Kiagus A Hadi [1,*], Anung Suwito [1]

[1]Machine Maintenance Department, PT Bukit Asam Tbk, Jalan Soekarno Hatta KM 15, Tarahan, Srengsem, Panjang, Bandar Lampung, 35243, Indonesia
[*]Corresponding author: abdulhadi_kiagus@yahoo.com; Tel.: +62- 85269339103

Abstract: Fatigue failure due to impact loads on the CV507 screen coal flow breaker plate has caused operational constraints that hamper coal production at PT. Bukit Asam – Tarahan Harbor. This research aims to determine the optimal material selection for coal flow breaker plates to achieve superior fatigue life and operational safety. HB400 material was selected for its high hardness and wear resistance, suitable for applications experiencing friction and direct coal impact. GS20Mn5 was chosen for its high toughness and superior impact energy absorption capabilities without cracking, particularly under repeated impact loading conditions. Two materials, Hardock (HB400) and GS20Mn5, with thicknesses of 15 mm and 20 mm respectively, were analyzed using static structural and explicit dynamic analysis in ANSYS Workbench 2022 R1 software. Simulation results indicate that the maximum operational impact load is 15.2 kN. The highest maximum Von Mises stress occurred in the Hardock (HB400) material with 15 mm thickness at 2348.3 MPa, with total deformation of 12.139 mm. Increasing thickness by 5 mm in the Hardock (HB400) material reduced stress and total deformation to 1543.3 MPa and 11.476 mm, respectively. GS20Mn5 material with 20 mm thickness demonstrated the longest fatigue life of 8 months compared to Hardock (HB400). This research provides material selection guidelines for coal flow breaker plates, offering significant value for engineering applications and the mining industry.

Keywords: Coal screening; Fatigue life; Impact loading; Finite element analysis; Material selection

1. Introduction

The utilization of coal as boiler fuel for electrical energy generation in Steam Power Plants (PLTU) remains dominant and irreplaceable in the global energy sector. According to Afin and Kiono (2021), it is projected that coal consumption will continue to dominate until 2050, amounting to 301 million tons of oil equivalent (TOE) under the Business As Usual (BAU) scenario, with only a 4% decrease from 2040 levels [1]. Coal processing operations involve several critical machine units, including rotary car dumpers, stacker reclaimers, crushers, vibrating screens, barge loaders, and shiploaders. Among these units, the vibrating screen is equipped with a flow breaker plate component (outflow reducer) that functions as a filter or separator for oversized coal particles. The vibrating screen

DOI: https://doi.org/10.24853/sintek.19.1.25-41
Received February 2025; Revised March 2025; Accepted June 2025

component, known as the coal flow breaker plate, frequently experiences failure due to impact loading caused by coal dropping from a height of 5 meters. Figure 1 illustrates the typical damage patterns observed in these components.

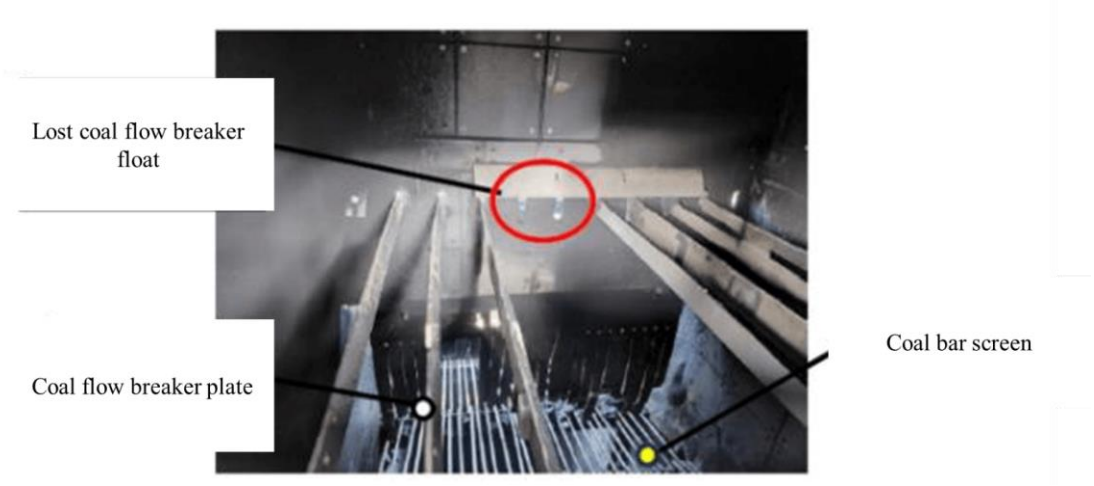

Figure 1. The Coal Flow Breaker Plate on the Vibrating Screen Component is Damaged.

Impact-induced damage in structural components and machinery has become a major research focus. Cherukara and Yeddu (2024) investigated the performance of Formula 1 race cars under impact loads using finite element simulation, demonstrating that maximum von Mises stress remained below yield stress, indicating no material failure under the applied impact conditions [2]. Similarly, Yusnayadi et al. (2019) conducted comprehensive impact testing on go-kart chassis using explicit dynamic analysis with speed variations from horizontal directions, evaluating total deformation distribution, von Mises stress, and safety factors. Their findings identified AISI 1020 material as the optimal choice for safe operation up to 10 km/h [3]. Fatigue life analysis through computational methods has also gained significant attention. Maulana et al. (2022) analyzed von Mises stress, safety factors, and fatigue characteristics of coconut fiber chopping machines using Autodesk Inventor software [4].

This research distinguishes itself from previous studies by implementing a coupled analytical approach, combining Static Structural Analysis and Explicit Dynamic simulation within a single computational framework. Additional differentiating factors include unique geometric configurations, specific material types, operational loading conditions, and comprehensive fatigue life assessment. Engineering component performance evaluation must consider multiple criteria including structural strength, quality assurance, operational comfort, economic viability, and aesthetic considerations [5], [6], [7]. Material selection involves systematic investigation of candidate materials and comprehensive evaluation of their characteristics to ensure optimal material-application matching. For successful implementation, materials must exhibit predictable and reliable behavior under service conditions [8]. Computational modeling represents one of the most efficient and cost-effective approaches for performance assessment of components with different material configurations.

This investigation focuses on two high-performance materials: HB400 and GS20Mn5. HB400 (Hardox 400) is renowned for exceptional wear and impact resistance, making it particularly suitable for harsh mining environments. Its high tensile strength and resistance to plastic deformation make it ideal for handling dynamic loads commonly encountered in coal flow breaker plate applications [9]. Additionally, HB400 exhibits superior corrosion-resistant properties, which are crucial for extending fatigue life under environmental conditions containing corrosive elements [10].

GS20Mn5 represents a manganese-alloyed steel with excellent impact and fatigue load resistance. The manganese content enhances both strength and wear resistance characteristics. Previous mining applications of GS20Mn5 have demonstrated its capability to withstand extremely challenging operational conditions, including exposure to abrasive particles and heavy loading [11]. The superior mechanical properties of GS20Mn5, particularly its high toughness and tensile strength, make it an excellent candidate for fatigue-critical applications [12].

Recent decades have witnessed extensive experimental and computational studies utilizing explicit dynamic analysis concepts [13]. Impact testing using ANSYS Explicit Dynamics enables determination of material shock resistance characteristics, including brittleness induced by heat treatment, casting defects, and geometric influence factors [14][15]. Conversely, finite element analysis of structures and components under static conditions is effectively accomplished using ANSYS Static Structural, which provides comprehensive capabilities including geometry modeling, material definition, meshing, boundary condition specification, loading application, structural analysis, visualization, and reporting.

The critical impact load of 15.2 kN identified in this study represents a fundamental parameter in coal flow breaker plate applications, particularly in the context of fatigue failure mechanisms. In mining operations, coal flow breaker plates are subjected to extreme loading conditions, including repetitive impact loads from falling coal material. Excessive impact loading can initiate crack formation and micro-damage within the material structure. Research indicates that high-magnitude impact loads can compromise material porosity and internal structure integrity, potentially reducing wear and fatigue resistance [16]. In coal flow breaker plate applications, such damage accelerates wear processes and reduces component fatigue life, resulting in increased maintenance costs and decreased production efficiency [17].

This research was conducted to extend the operational life of the CV507 screen coal flow breaker plate at PT. Bukit Asam Tarahan Port through optimal material selection based on comprehensive simulation results using Finite Element Analysis with ANSYS Workbench 2022 R1 Static Structural and Explicit Dynamic modules. The research presents innovative elements and novelty in coal flow breaker subsystem analysis, determining optimal, effective, and efficient materials for mitigating fatigue impact failures caused by coal discharge loads utilizing materials available at PT. Bukit Asam Tbk. The selected material is expected to demonstrate significantly extended service life. The research outcomes provide substantial added value for both engineering science advancement and mining industry applications.

2. Methods

Static structural and explicit dynamic analyses were conducted on coal flow breaker plates to evaluate material performance under operational loading conditions. Two high-performance materials were investigated: Hardox (HB400) and GS20Mn5, with geometric specifications of 1500 mm length, 200 mm width, and variable plate thicknesses of 15 mm and 20 mm. The coal drop height was established at 5000 mm based on actual operational conditions at the facility. The mechanical properties of both materials are presented in Table 1, which served as fundamental input parameters for the finite element analysis. Simulation outcomes include total deformation, Von Mises stress distribution, and fatigue life cycles, determined using ANSYS Workbench Explicit Dynamic and Static Structural 2022 R1 software to assess the durability and performance characteristics of each material configuration.

2.1 Data Collection and Site Characterization

Parameter input data collection was conducted at PT. Bukit Asam Tbk Tarahan Port Unit, Bandar Lampung, which serves as Indonesia's largest commercial coal terminal with ship accommodation capacity up to 210,000 dead-weight tonnage (DWT). All operational values were systematically obtained and subsequently entered into the engineering data module for computational analysis.

Simulation and analytical procedures were performed in the Structural Mechanics Laboratory, Department of Mechanical Engineering, Faculty of Engineering, University of Lampung, ensuring controlled environmental conditions and computational accuracy.

2.2 Material Properties and Selection Criteria

Table 1. Mechanical properties of test materials (DIN 17100, ASTM)

Material properties	Symbol	Material	
		GS20 Mn5	Hardock (HB400)
Tensile Strength (MPa)	Sut	570	1250
Yield Strength (MPa)	Ys	225	345
Young Modulus (GPa)	*E*	210	210
Density (Kg/m³)	ρ	7,820	7,473
Poisson Ratio	v	0.29	0.29

The GS20Mn5 material exhibits a tensile strength (Sut) of 570 MPa and yield strength (Ys) of 225 MPa, while Hardox (HB400) demonstrates significantly higher tensile strength of 1250 MPa and yield strength of 345 MPa. Both materials share identical Young's modulus values of 210 GPa, indicating equivalent stiffness characteristics. Density variations require consideration, with GS20Mn5 having a density of 7,820 kg/m³ compared to Hardox (HB400) at 7,473 kg/m³. Both materials exhibit similar Poisson's ratio values of 0.29, enabling relatively consistent deformation distribution under applied stress conditions. The selection of GS20Mn5 offers advantages in applications requiring enhanced dynamic properties and resilience characteristics [18].

2.3 Fatigue Properties Calculation

Additional material properties were calculated using established engineering formulations [19]:

Fatigue strength coefficient:

$$\sigma' f = S_{ut} + 345\ MPa \tag{1}$$

where the constant 345 MPa represents the standard fatigue strength enhancement factor [19].

Fatigue strength exponent:

$$b = -\frac{\log(\frac{\sigma' f}{S' e})}{\log(2N_e)} \tag{2}$$

Fatigue ductility coefficient:

$$\varepsilon' f = 0.812 - 74\ x\ {}^{S_u}/_{E} \tag{3}$$

Cyclic strength coefficient:

$$K' = \frac{\sigma' f}{(\varepsilon' f)^{n'}} \tag{4}$$

Cyclic hardening exponent:

$$n' = \frac{b}{c} \tag{5}$$

Endurance strength:

$$Se' = 0.5\ x\ S_{ut} \tag{6}$$

2.4 Impact Load Determination

The impact load was determined based on the mass of coal falling on the transverse surface of the flow breaker plate, measured using a calibrated load cell installed on the component. The impact force calculation follows Newton's second law:

$$F = m.g \tag{7}$$

where F represents the maximum impact load (kN), m denotes the mass of falling coal (kg), and g is the gravitational acceleration (9.81 m/s²).

2.5 Finite Element Analysis Procedure

Fatigue life assessment was conducted using ANSYS Static Structural, which analyzes material fatigue behavior until fracture conditions are reached through computational simulation. The resulting data generates S-N (Stress-Number of cycles) curves for comprehensive fatigue characterization [20]. The computational workflow for ANSYS Workbench Explicit Dynamic and Static Structural 2022 R1 simulation is illustrated in Figure 2.

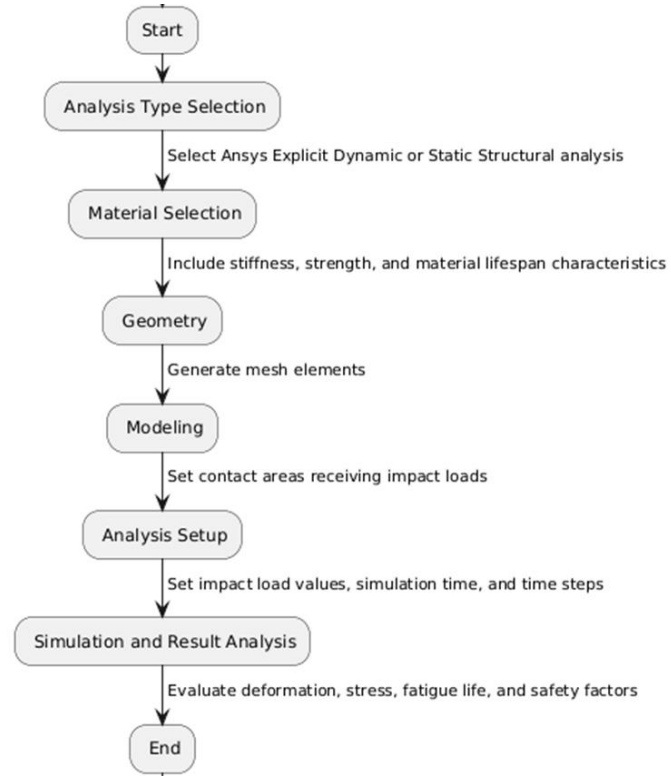

Figure 2. ANSYS Workbench Explicit Dynamic and Static Structural 2022 R1 simulation flowchart

Stress and deformation distributions were obtained from tabular data generated by ANSYS Workbench 2022 R1 analysis. The fatigue life graphs and S-N (Stress-Number of Cycle) curves were constructed following ASTM E647 [21] standards through the following systematic procedure:

- Manual tabular data creation from ANSYS Workbench fatigue life analysis results (Stress and Number of Cycle)
- Logarithmic transformation of tabular data using Microsoft Excel
- N-S curve generation from logarithmic data (Number of Cycle vs. Stress)
- Trendline analysis displaying equation and regression coefficient values
- Equation substitution with values x = Log N and y = log σ
- S-N curve equation derivation**: σ = A × N^x
- Tabular data reconstruction from initial stress values using the derived equation σ = A × N^x
- Graph generation based on reconstructed tabular data following ASTM E647 guidelines
- Validation confirmation through trendline regression values approaching unity, indicating acceptable simulation accuracy

2.6 Fatigue Life Calculation Methodology

Fatigue life calculations were performed by correlating the cycle average fatigue life of each specimen with actual impact data collected during operational monitoring. Initial data collection revealed 4 impacts occurring every 15 minutes, resulting in 384 impacts per operational day. The fatigue life calculation methodology follows:

Fatigue life (days):

$$fatigue\ life\ (days) = \frac{cycle\ average\ fatigue\ life}{impact\ (days)} \tag{8}$$

Fatigue life (months):

$$fatigue\ life\ (months) = \frac{cycle\ average\ fatigue\ (days)}{30} \tag{9}$$

This methodology provides practical engineering estimates for maintenance scheduling and component replacement planning in actual mining operations.

2.7 Mesh Convergence and Boundary Conditions

The finite element meshing parameters were initially set to default configurations, followed by iterative convergence analysis to determine optimal meshing characteristics. Convergence criteria required error values below 0.05 to ensure computational accuracy. Boundary conditions included fixed support constraints at plate ends and centralized impact loading of 15.2 kN, representing actual operational conditions at the coal screening facility.

3. Results and Discussion

3.1. Meshing and Boundary Conditions

The meshing parameters for the finite element model were initially set to default. Following the initial analysis, a mesh convergence study was conducted to determine the optimum mesh size that ensures result accuracy while maintaining computational efficiency. The final, converged mesh parameters yielded an error value below the acceptable threshold of 0.05. The boundary conditions, as illustrated in Figure 3, consisted of a Fixed Support constraint applied at both ends of the plate and a Pressure load of 30 MPa, corresponding to the calculated impact force of 15.2 kN. This force was derived from the measured mass of falling coal (m = 1,550.21 kg) using Equation 7 (F = m·g),

which is consistent with the operational conditions observed at the PT Bukit Asam Tarahan Port facility.

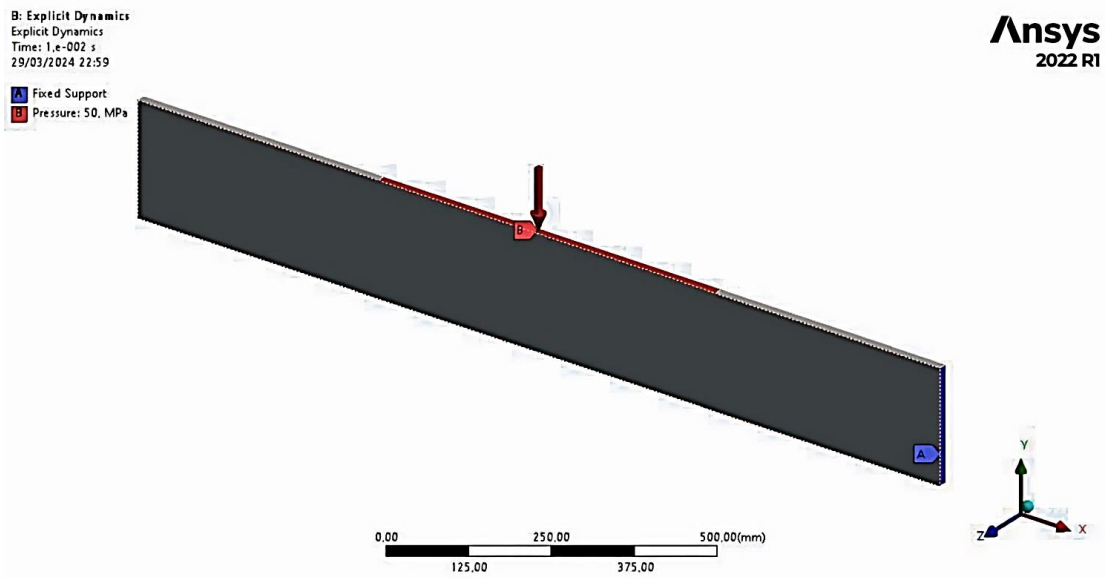

Figure 3. Boundary Condition Parameter Input

3.2. Stress Distribution and Deformation Analysis

The equivalent von Mises stress distributions for all four material and thickness configurations are presented in Figure 4. The results indicate a consistent pattern where the maximum stress is concentrated at the edges of the plate, adjacent to the fixed supports. This phenomenon is a classical result of stress concentration and the restraining effect of the boundary conditions [22], [23]. When a load is applied to the center of a plate with fixed ends, the edges experience significant bending moments and reaction forces, leading to localized stress intensification [24].

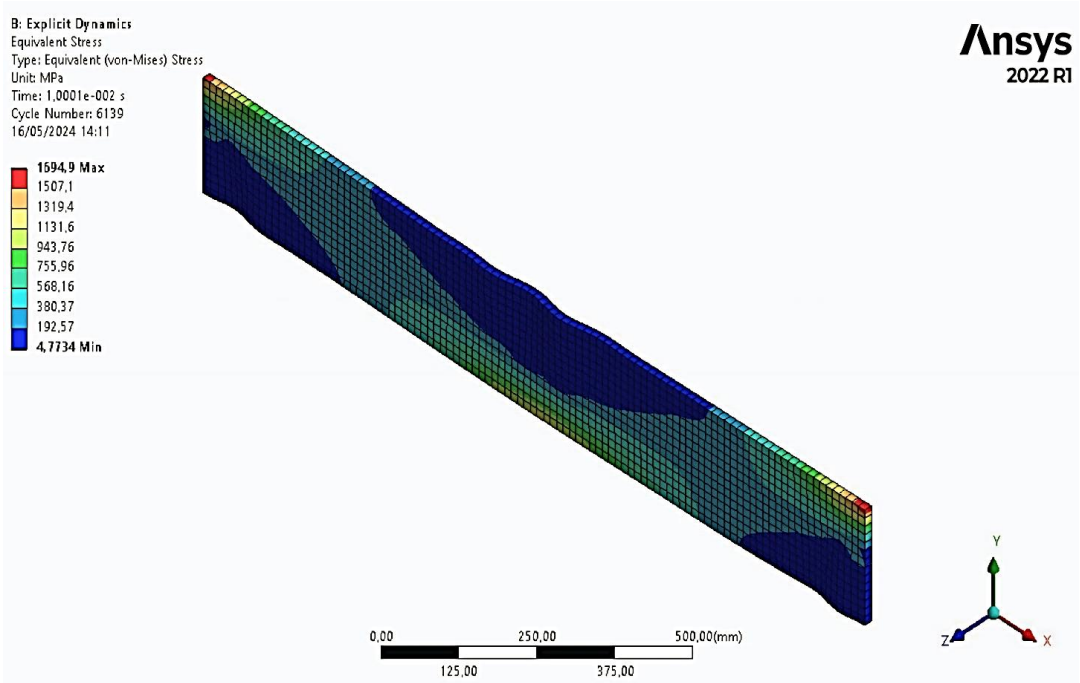

a). GS20 Mn5 with 15 mm plate thickness

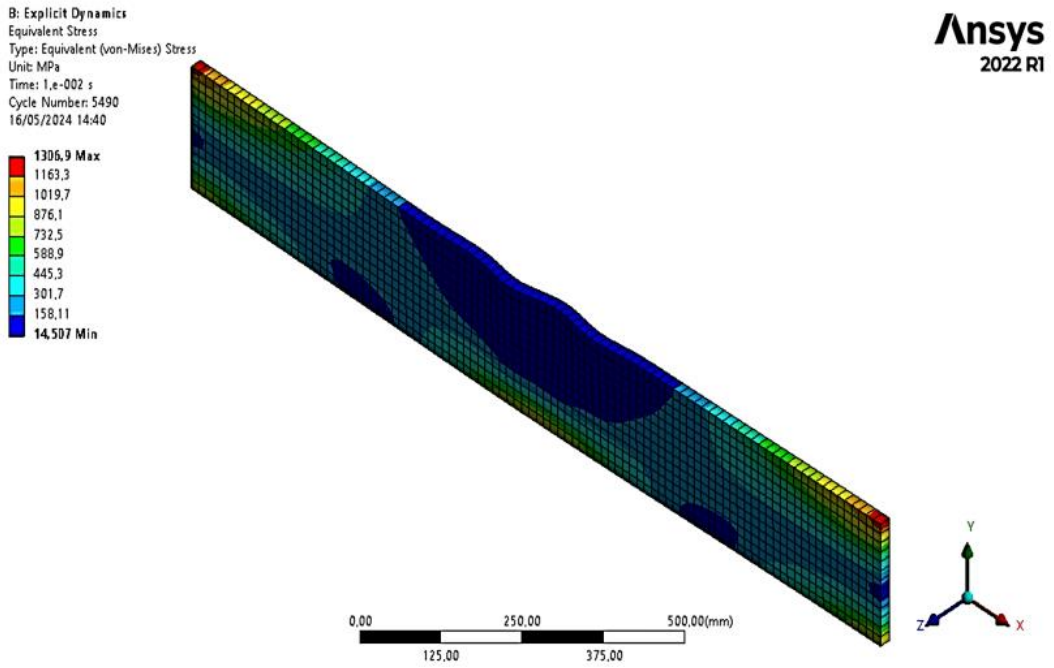

b). GS20 Mn5 with 20 mm plate thickness

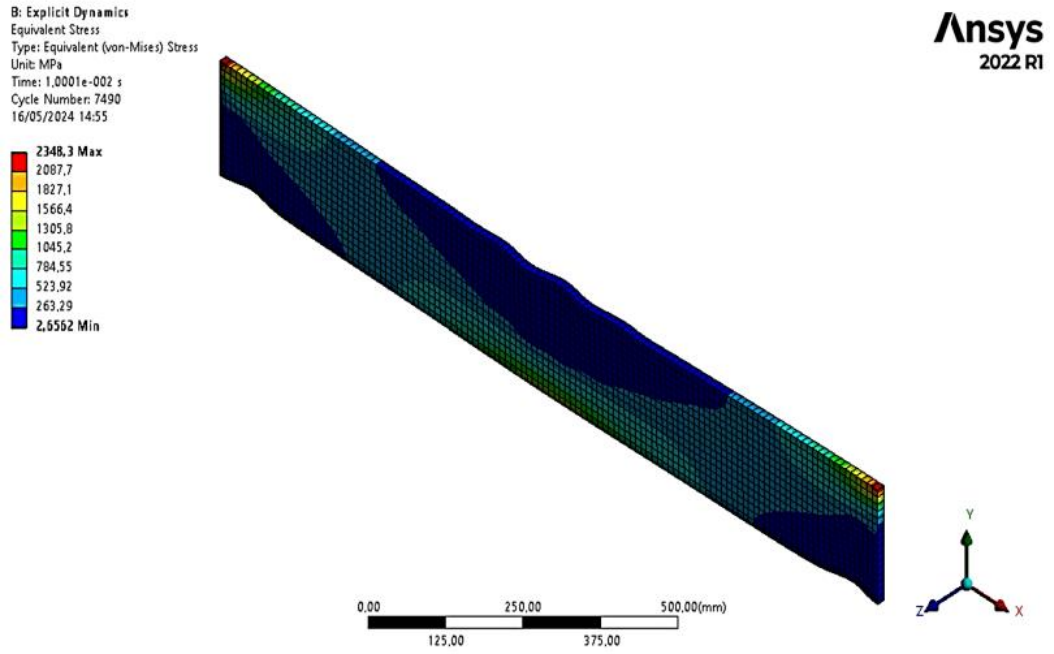

c). Hardock (HB400) with 15 mm plate thickness

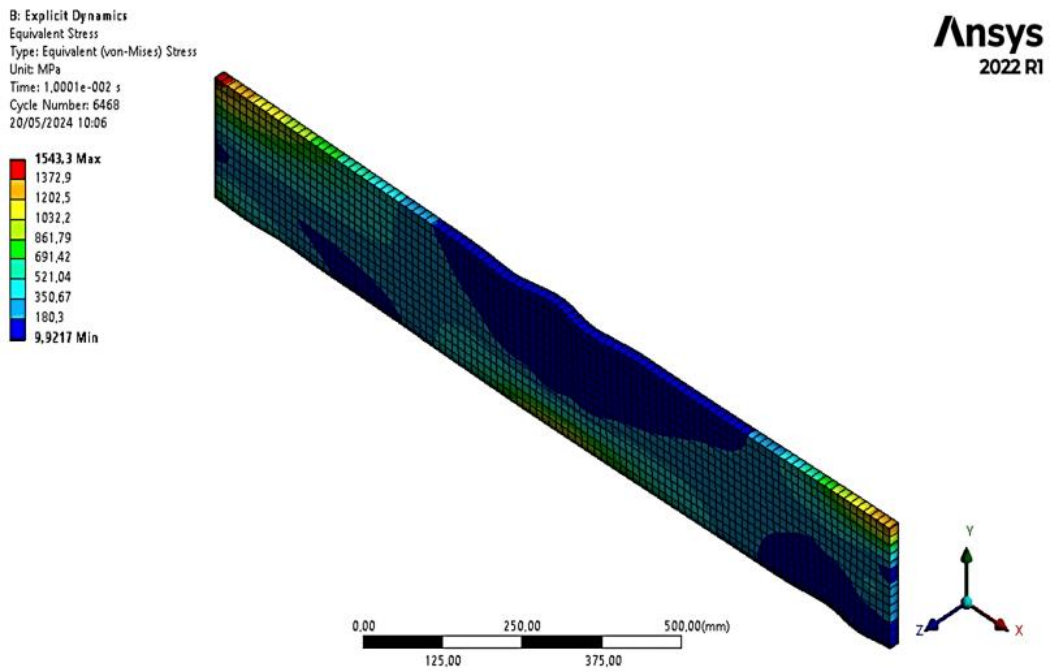

d). Hardock (HB400) with 20 mm plate thickness

Figure 4. Von Mises Stress Graph

The quantitative maximum stress values are summarized in Table 2. The simulation revealed that the Hardox (HB400) material with a 15 mm thickness sustained the highest stress (2348.3 MPa), far exceeding its yield strength (345 MPa) and indicating a high probability of plastic deformation or failure. In contrast, the GS20 Mn5 material with a 20 mm thickness exhibited the lowest maximum stress (1306.9 MPa).

Table 2. Comparison of the Maximum Stress, Deformation, and Fatigue Life

Material Type	Dimensions			σ Max. (MPa)	Deformation (mm)	Fatigue Life	
	l (mm)	b (mm)	h (mm)			Day	Month
Hardock (HB400)	1500	15	200	2348,3	12,193	194,20	6,47
	1500	20	200	1543,3	11,476	232,19	7,76
GS20 Mn5	1500	15	200	1694,9	11,586	214,33	7,14
	1500	20	200	1306,9	10,942	239,87	8,00

A critical finding is the significant effect of increasing plate thickness. The addition of 5 mm of thickness resulted in a substantial reduction in stress for both materials. The stress was reduced by 22.9% (from 1694.9 MPa to 1306.9 MPa) for GS20 Mn5 and by 34.3% (from 2348.3 MPa to 1543.3 MPa) for Hardox (HB400). This reduction is mechanically explained by the fundamental relationship between stress (σ), force (F), and cross-sectional area (A) ($\sigma = F/A$). Increasing the thickness increases the cross-sectional area, thereby reducing the induced stress for a constant applied load [24]. The stress distribution received at the longitudinal region of the plate is shown in Figure 5.

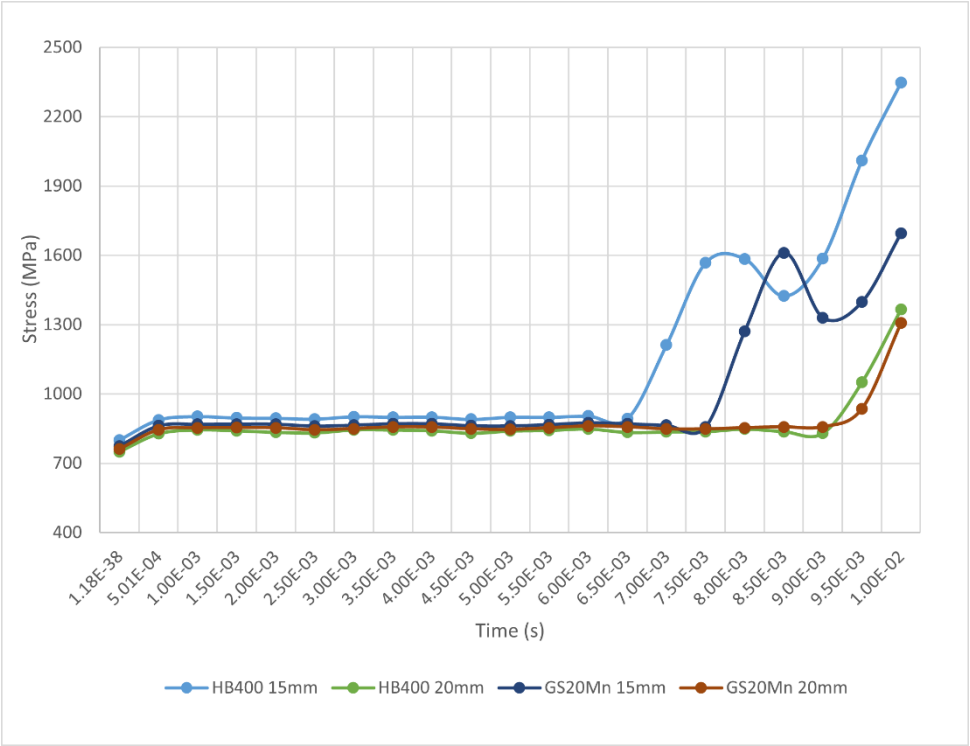

Figure 5. Comparison of Stress Graphs of GS20 Mn5 vs Hardock (HB400) Materials with thicknesses of 15 mm and 20 mm

The total deformation results, shown in Figure 6, correlate directly with the stress findings. The deformation was highest for the 15 mm thick Hardox (HB400) plate (12.129 mm) and lowest for the 20 mm thick GS20 Mn5 plate (10.942 mm). The deformation pattern consistently showed the maximum deflection at the center point of the plate, which aligns with the expected deformation mode of a beam or plate under a central point load with fixed ends [25]. By knowing the maximum deformation of different materials and thicknesses, it can be determined which material and size is the safest and strongest to withstand the load [26], [27], [28], [29]. The reduction in deformation with increased thickness further confirms the enhanced structural stiffness and load-bearing capacity offered by the 20 mm plates.

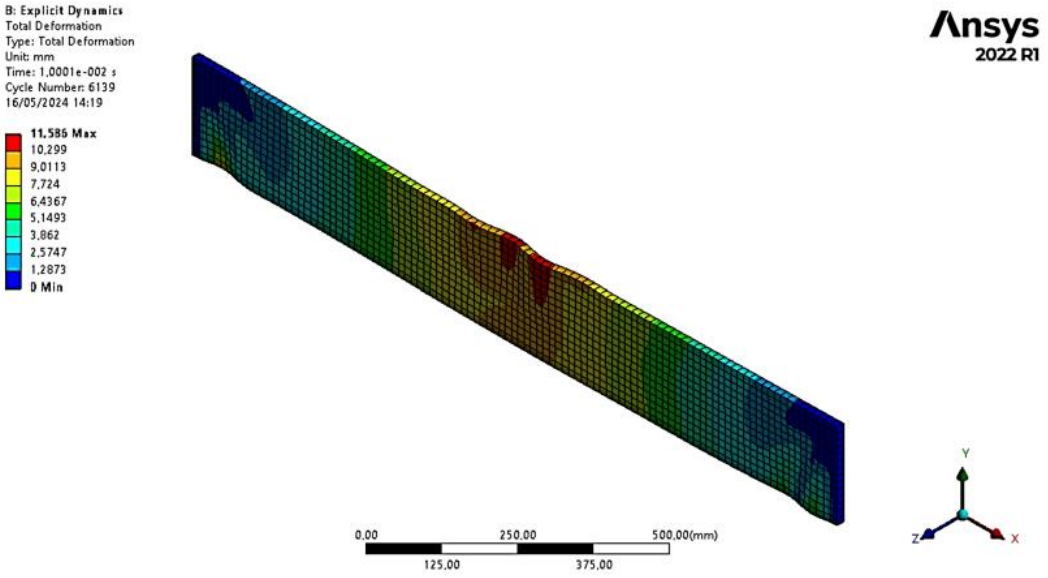

a). GS20 Mn5 with 15 mm plate thickness

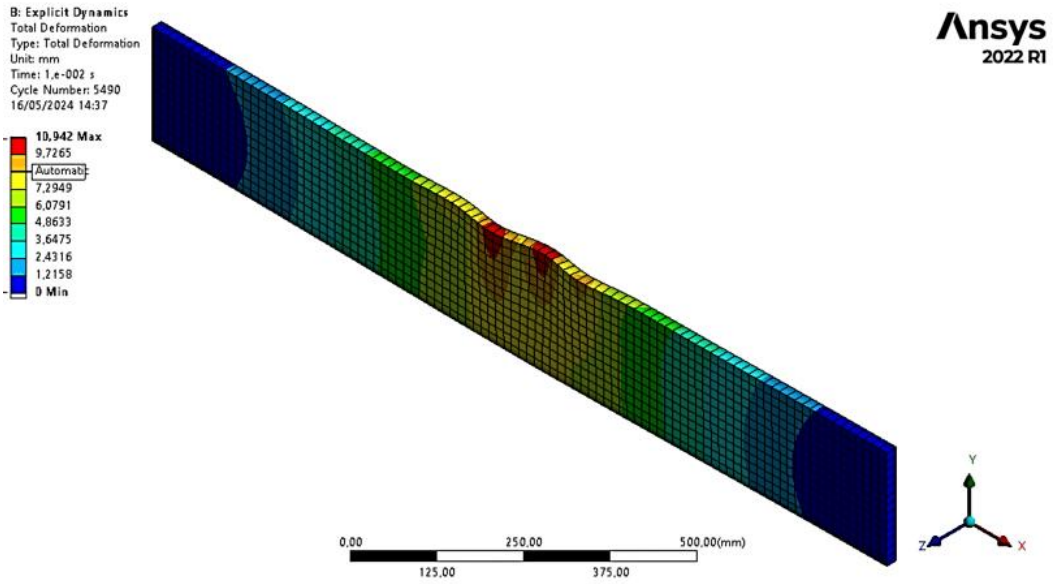

b). GS20 Mn5 with 20 mm plate thickness

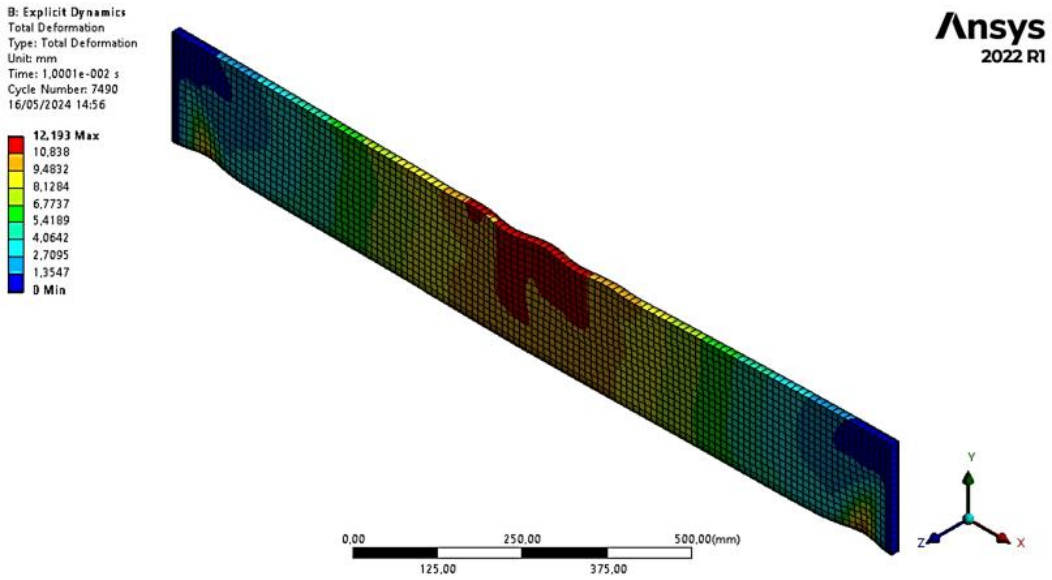

c). Hardock (HB400) with 15 mm plate thickness

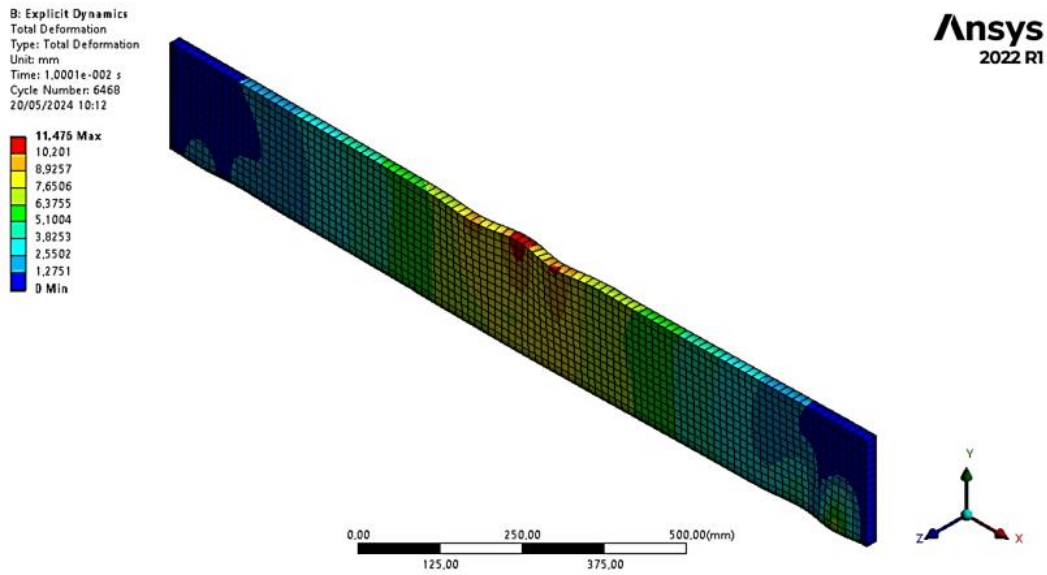

d). Hardock (HB400) with 20 mm plate thickness

Figure 6. Deformation Result of Test Material

3.3. Fatigue Life Evaluation

The fatigue life analysis, based on the stress results and the methodology outlined in Section 2, provides the most critical insight for material selection. The fatigue life contours are displayed in Figure 7, with areas of minimum life (indicating potential crack initiation sites) shown in bright red, primarily located at the supported edges and the impact point in the center. This distribution confirms that stress concentration zones are the primary drivers for fatigue crack initiation [30].

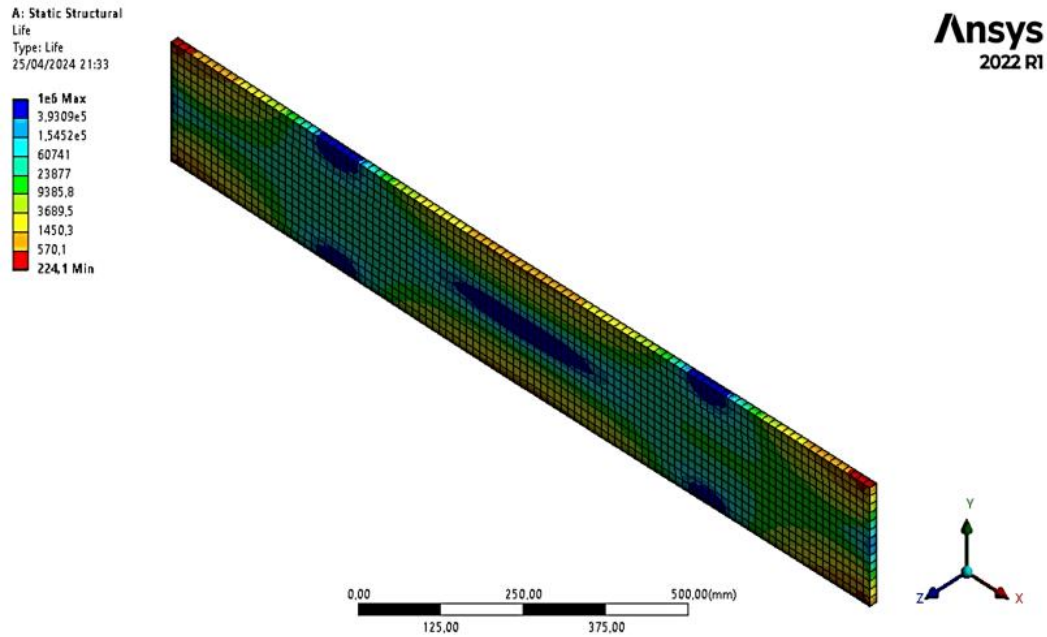

a). GS20 Mn5 with 15 mm plate thickness

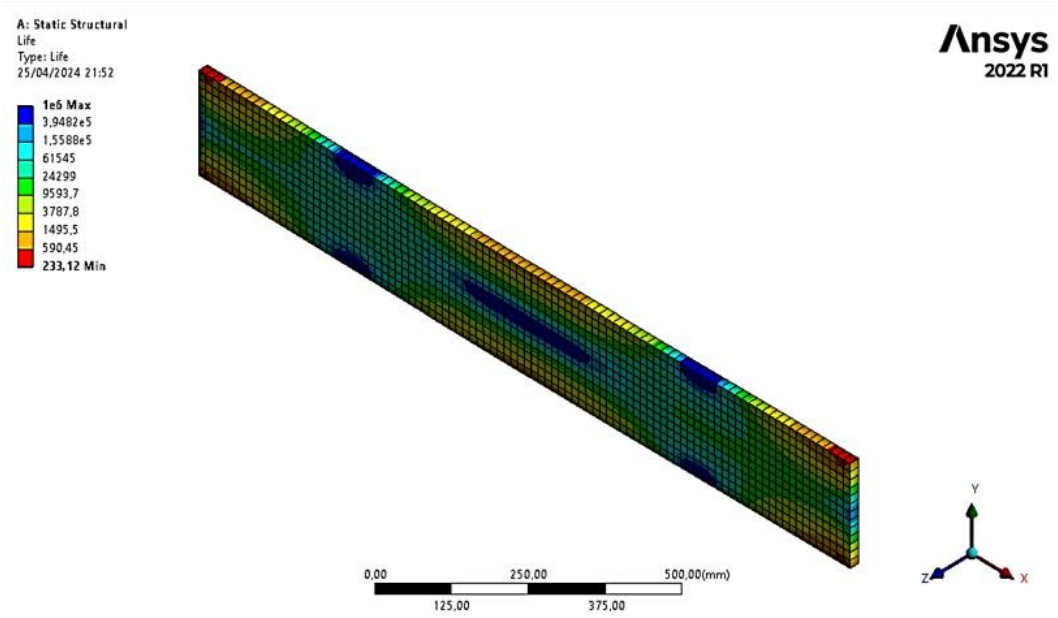

b). GS20 Mn5 with 20 mm plate thickness

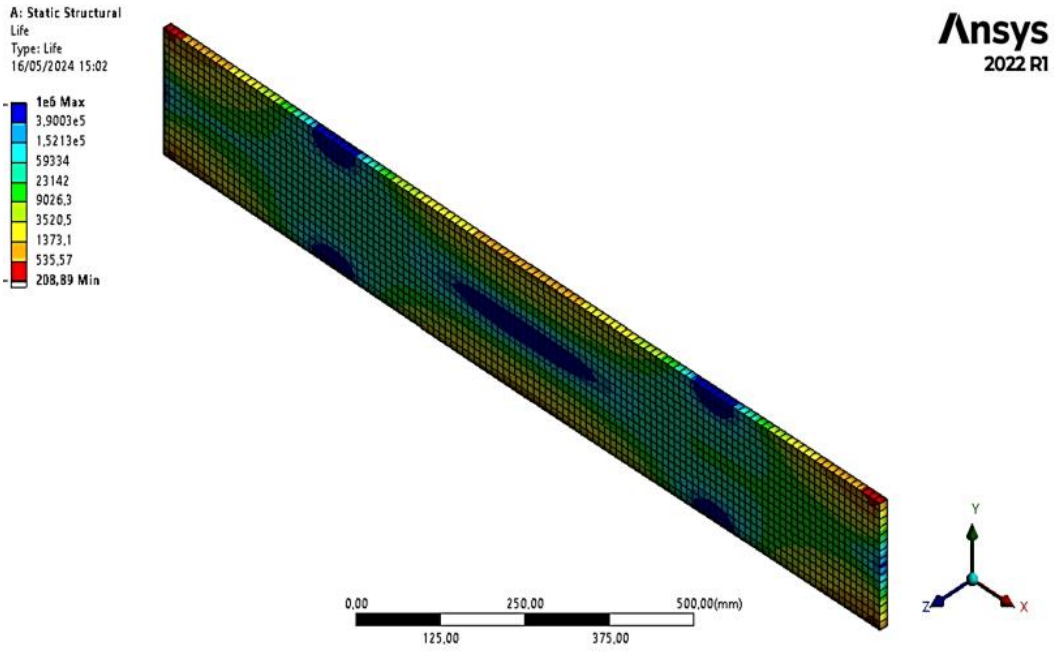

c). Hardock (HB400) with 15 mm plate thicknes

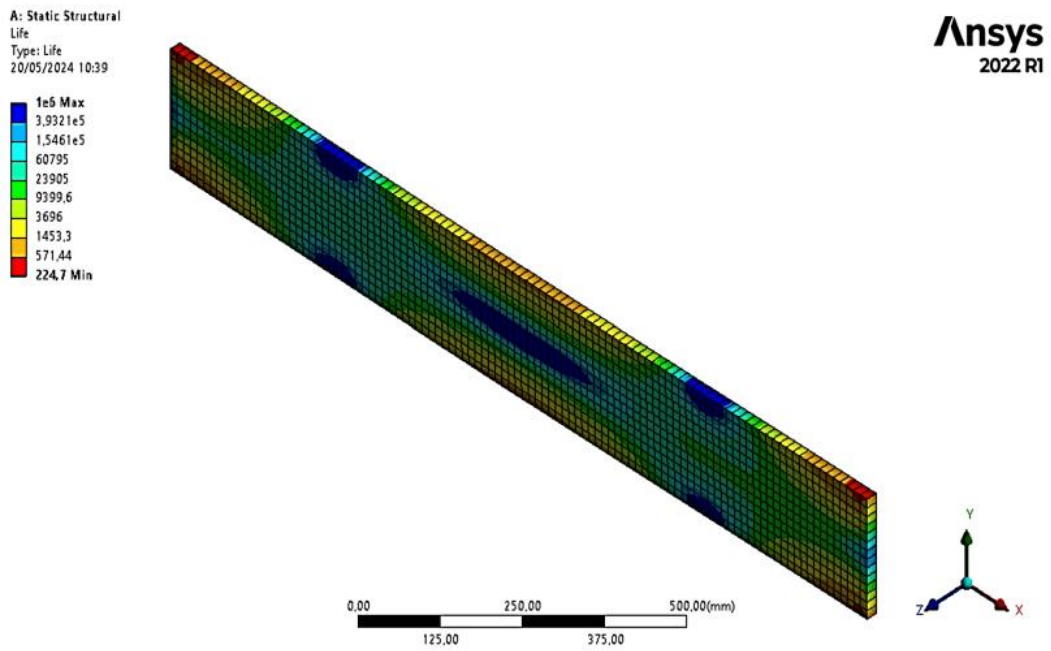

d). Hardock (HB400) with 20 mm plate thickness

Figure 7. Fatigue Life Color Contours

The calculated average cycles to failure and the resulting service life in months are presented in Table 3. The conversion from cycles to months was based on recorded operational data of 384 impacts per day. The results demonstrate that the GS20 Mn5 material with a 20 mm thickness offers the longest service life of 8.00 months. This is notably longer than its 15 mm counterpart (7.14 months) and both configurations of the harder Hardox (HB400) material (7.76 months for 20 mm and 6.47 months for 15 mm). The Stress (S) to Number of Cycle (N) curve of each test to determine fatigue life is shown in Figure 8.

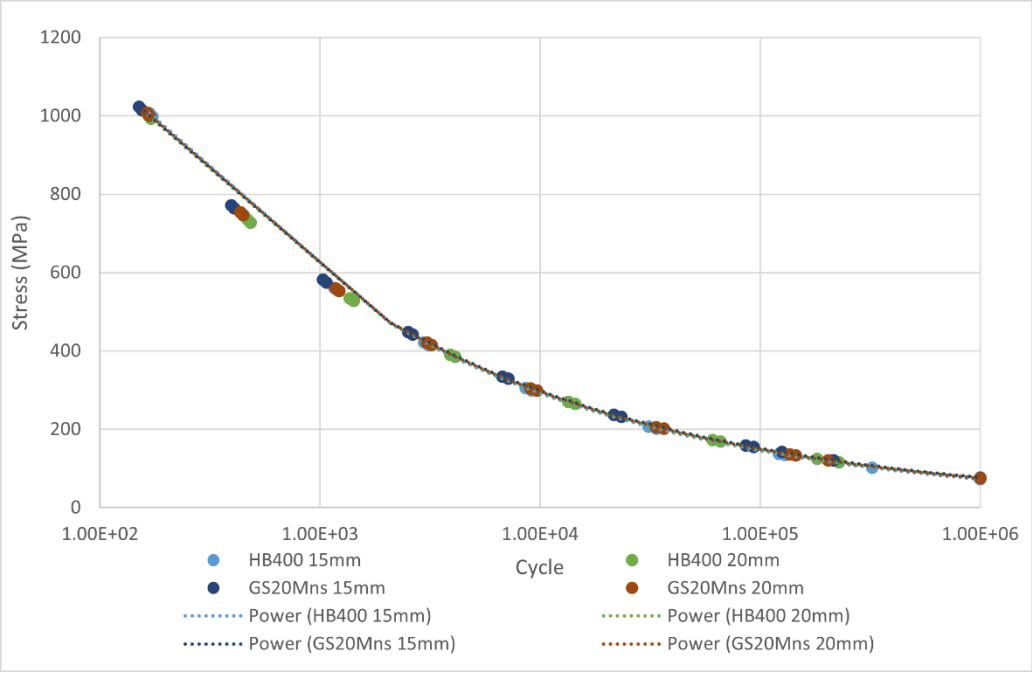

Figure 8. Comparison of S-N Curves of Test Materials

This outcome can be attributed to the superior toughness and microstructural properties of GS20 Mn5. While Hardox (HB400) possesses higher tensile and yield strength, its lower toughness makes it more susceptible to crack initiation and propagation under high-impact, cyclic loading. The manganese content in GS20 Mn5 promotes a more homogeneous and stable austenitic microstructure, which enhances its ability to absorb impact energy and resist the initiation and growth of fatigue cracks [31], [32]. Furthermore, materials with finer and more uniform microstructures are known to exhibit better fatigue resistance, as they provide a more effective barrier to crack propagation [33], [34], [35]. The high R^2 values (all above 0.98) for the S-N curve fittings validate the reliability of the fatigue life predictions.

Table 3. Fatigue Life for Each Material

Material Type	Thickness	Cycle average	*Impact*/ Day	*Fatigue Life* (Month)
GS20 Mn5	15 mm	82303	384	7.14
	20 mm	92109	384	8.00
Hardock (HB400)	15mm	74572	384	6.47
	20mm	89350	384	7.76

3.4. Practical Implications and Cost-Benefit Analysis

The selection of GS20 Mn5 with a 20 mm thickness is not only technically superior but also economically and environmentally justified. Although the initial material cost may be higher than conventional alternatives like ST37, the extended service life directly reduces the frequency of unplanned downtime, maintenance, and component replacement. This leads to significant long-term cost savings, estimated in this study at over 47 million IDR per component lifecycle. Additionally, the longer lifespan contributes to sustainability by reducing waste generation and the energy consumption associated with manufacturing and transporting replacement parts.

4. Conclusions

This study successfully employed finite element analysis (FEA) to evaluate the fatigue impact performance of HB400 and GS20 Mn5 as candidate materials for the coal flow breaker plate at PT Bukit Asam Tarahan Port. Through a combination of static structural and explicit dynamic simulations in ANSYS, the operational impact load was quantified at 15.2 kN, and the stress, deformation, and fatigue life for two thicknesses (15 mm and 20 mm) of each material were comprehensively analyzed.

The results demonstrate that material selection is a critical trade-off between hardness and toughness. While the Hardox (HB400) material exhibited higher tensile strength, the GS20 Mn5 alloy, characterized by its high manganese content and superior toughness, proved more effective in withstanding repeated impact loads. The GS20 Mn5 plate with a 20 mm thickness was identified as the optimal choice, exhibiting the lowest maximum von Mises stress (1306.9 MPa), the smallest total deformation (10.942 mm), and the longest fatigue life (8.00 months). Increasing the plate thickness from 15 mm to 20 mm was a highly effective design modification, reducing stress by 22.9% for GS20 Mn5 and 34.3% for HB400, thereby significantly extending the service life of both materials.

Therefore, it is conclusively recommended to implement GS20 Mn5 with a 20 mm thickness for the coal flow breaker plate. This selection provides a technically superior solution that enhances operational reliability by reducing unplanned downtime and maintenance frequency. Furthermore,

it offers substantial economic benefits through long-term cost savings and aligns with sustainable practices by minimizing waste and the environmental footprint associated with frequent component replacement. For future work, experimental validation of these simulation results and the incorporation of environmental factors, such as corrosion, into the model are recommended to further refine the prediction accuracy.

Acknowledgments

The authors gratefully acknowledge the support and facilities provided by the Mechanical Engineering Laboratory, Department of Mechanical Engineering, Faculty of Engineering, Universitas Lampung. We also extend our sincere gratitude to the management and engineers of PT Bukit Asam Tbk, Tarahan Port Unit, Bandar Lampung, for their invaluable cooperation, granting access for data collection, and providing essential operational insights that made this research possible.

Conflict of Interest

The authors declare no conflicts of interest.

References

[1] A. P. Afin and B. F. T. Kiono, "Potensi energi batubara serta pemanfaatan dan teknologinya di Indonesia tahun 2020 - 2050: Gasifikasi batubara," *J. Energi Baru Dan Terbarukan*, vol. 2, no. 2, pp. 114–122, 2021, doi: 10.14710/jebt.2021.11429.

[2] M. J. Cherukara and H. K. Yeddu, "Finite element analysis of F1 car chassis under impact loading," in *Proc. Struct. Integr.*, vol. 42, 2022, pp. 1234–1241. doi: 10.1016/j.prostr.2022.12.156.

[3] M. M. Yusnayadi, B. Hartono, U. Ibn, and K. Bogor, "Analisa uji impact chassis gokart berbasis kecepatan," *J. AlMikanika*, vol. 1, no. 4, 2019, doi: 10.32832/almikanika.v1i4.5194.

[4] A. P. Maulana, "Analisis fatigue menggunakan Autodesk inventor," *J. Tek. Mesin Produksi*, vol. 3, no. 1, pp. 17–22, 2022.

[5] G. Singh, "A review on effect of heat treatment on the properties of mild steel," *Mater. Today Proc.*, vol. 26, pp. 1–3, 2020, doi: 10.1016/j.matpr.2020.07.702.

[6] M. Jia, P. Hu, X. Zhang, and G. Hu, "Rust conversion of proanthocyanidins to archaeological steel: A case study of Lingzhao Xuan in the Forbidden City," *Molecules*, vol. 27, no. 22, p. 7711, 2022, doi: 10.3390/molecules27227711.

[7] B. G. Tentua, "Analisa kelelahan velg racing Toyota Avansa dengan menggunakan metode element hingga," *J. Arika*, vol. 9, no. 1, pp. 63–69, 2015, [Online]. Available: https://ojs3.unpatti.ac.id/index.php/arika/article/view/415

[8] W. P. Spence and E. Kultermann, *Construction Materials, Methods and Techniques*, 4th ed. Boston, MA, USA: Cengage Learning, 2016.

[9] P. Krawczyk and A. Śliwińska, "Analysis of the impact of material properties on the wear rate of mining machinery components," *Arch. Min. Sci.*, vol. 65, no. 2, pp. 345–358, 2020, doi: 10.24425/ams.2020.134141.

[10] A. Chmiela, "The analysis of the structure of mining plants liquidation outlays," *Eur. J. Bus. Manag. Res.*, vol. 8, no. 3, pp. 204–214, 2023, doi: 10.24018/ejbmr.2023.8.3.1946.

[11] R. Juniah, "Study of carbon value of the allotment of former coal mining land of PT Samantaka Batubara for sustainable mining environment," *J. Sustain. Dev.*, vol. 11, no. 4, p. 213, 2018, doi: 10.5539/jsd.v11n4p213.

[12] A. Chmiela, J. Smoliło, and M. Gajdzik, "A multifaceted method of analyzing the amount of expenditures on mine liquidation processes in SRK S.A.," *Manag. Syst. Prod. Eng.*, vol. 30, no. 2, pp. 130–139, 2022, doi: 10.2478/mspe-2022-0016.

[13] M. A. P. Pratama, M. I. P. Hidayat, and R. Rochiem, "Analisa pengaruh ukuran partikel terhadap patahan gritcone pada vertical roller mill dengan simulasi explicit dynamic (Ls-Dyna)," *J. Tek. ITS*, vol. 6, no. 1, pp. F70–F75, 2017, doi: 10.12962/j23373539.v6i1.22907.

[14] D. Y. Kosasih, W. Anggono, and F. D. Suprianto, "Optimasi desain pelek mobil melalui simulasi pengujian impact sesuai standar SAE J175," *J. Meednnovah*, vol. 4, pp. 1–5, 2015.

[15] M. Nofri, "Analisis ketangguhan antara baja ST 37 dan ST 42 dengan ketebalan dan variasi lapisan karbon fiber untuk kerangka mobil listrik," *J. Presisi*, pp. 56–65, 2019.

[16] Y. Wang, Q. Han, and J. Yue, "Pore morphology changes and quantitative analysis and evaluation of high-rank coal samples after impact," *Energy Sci. Eng.*, vol. 12, no. 6, pp. 2519–2534, 2024, doi: 10.1002/ese3.1760.
[17] Z. Wang et al., "Research on the dynamic tensile characteristics and surface crack evolution of coal under impact loading," *Sci. Rep.*, vol. 14, no. 1, 2024, doi: 10.1038/s41598-024-64342-8.
[18] S. Jiang et al., "Study on the microstructure and mechanical properties of martensitic wear-resistant steel," *Crystals*, vol. 13, no. 8, p. 1210, 2023, doi: 10.3390/cryst13081210.
[19] R. G. Budynas and J. K. Nisbett, *Shigley's Mechanical Engineering Design*, 10th ed. New York, NY, USA: McGraw-Hill, 2015.
[20] D. Chandra, U. Budiarto, and H. E. Yudo, "Analisa teknis kekuatan dan perbandingan biaya material poros baling-baling kapal nelayan daerah Batang dengan menggunakan metode element hingga," *J. Tek. Perkapalan*, vol. 9, no. 4, pp. 334–342, 2021.
[21] S. Forth, J. C. Newman, and R. G. Forman, "Anomalous fatigue crack growth data generated using the ASTM standards," *J. ASTM Int.*, vol. 3, no. 3, Mar. 2006, doi: 10.1520/JAI13180.
[22] F. Rohman, D. Mardiyana, F. Ridha, and S. K. Damodar, "Structural analysis of waste separation machine frame using FEA method," *Int. J. Eng. Appl. Technol.*, vol. 6, no. 1, pp. 10–17, 2023, doi: 10.52005/ijeat.v6i1.80.
[23] X. Liu et al., "Comparison between novel anatomical locking guide plate and conventional locking plate for acetabular fractures: A finite element analysis," *Life*, vol. 13, no. 11, p. 2108, 2023, doi: 10.3390/life13112108.
[24] B. Sulaeman, "Modulus elastisitas berbagai jenis material," *PENA Tek. J. Ilm. Ilmu-Ilmu Tek.*, vol. 3, no. 2, p. 127, 2018, doi: 10.51557/pt_ijit.v3i2.176.
[25] H. Hao, T. T. Tran, H. Li, T. M. Pham, and W. Chen, "On the accuracy, reliability and controllability of impact tests of RC beams," Int. *J. Impact Eng.*, vol. 157, p. 103979, 2021, doi: 10.1016/j.ijimpeng.2021.103979.
[26] J. P. I. Kiswara, S. H. Suryo, and Muchammad, "Analisis kekuatan bucket dan gaya statis pada bucket backhoe John Deere 310I terhadap variasi material," *J. Tek. Mesin S-1*, vol. 11, no. 1, pp. 118–125, 2023, [Online]. Available: https://ejournal3.undip.ac.id/index.php/jtm.
[27] I. G. Kristanto, N. Mulyaningsih, and F. Hilmy, "Simulasi struktur rangka mesin pencacah sabut kelapa menggunakan software ANSYS Workbench," in *Seminar Nasional Teknik Mesin*, 2023, pp. 123–130.
[28] R. Effendi, R. Pratama, M. Qadri, and A. Y. Nasution, "Analysis of the frame design of cracker sheet printing and cutting machine using finite element method simulation," *J. Dinamis*, vol. 12, no. 1, pp. 7-13, 2024, doi: 10.32734/dinamis.v12i1.16359.
[29] B. Bickel et al., "Design and fabrication of materials with desired deformation behavior," *ACM Trans. Graph.*, vol. 29, no. 4, pp. 1–10, 2010, doi: 10.1145/1778765.1778800.
[30] E. Febriyanti, A. G. Abdul, and H. A. Suhartono, "Analisa kegagalan track link excavator," *Maj. Ilm. Pengkaj. Ind.*, vol. 12, no. 3, pp. 181–190, 2023, doi: 10.29122/mipi.v12i3.2886.
[31] J. Zghal, H. Gmati, C. Marcau, and F. Morel, "A crystal plasticity based approach for the modelling of high cycle fatigue damage in metallic materials," *Int. J. Damage Mech.*, vol. 25, no. 5, pp. 611–628, 2016, doi: 10.1177/1056789516650247.
[32] V. Igwemezie, A. Mehmanparast, and F. Brennan, "The influence of microstructure on the fatigue crack growth rate in marine steels in the Paris region," *Fatigue Fract. Eng. Mater. Struct.*, vol. 43, no. 10, pp. 2416–2440, 2020, doi: 10.1111/ffe.13312.
[33] X. Liu, Q. Wu, S. Su, and Y. Wang, "Evaluation and prediction of material fatigue characteristics under impact loads: review and prospects," *Int. J. Struct. Integr.*, vol. 13, no. 2, pp. 251–277, 2022, doi: 10.1108/IJSI-10-2021-0112.
[34] A. Yadollahi, M. Mahmoudi, A. Elwany, H. Doude, L. Bian, and J. C. Newman, "Fatigue-life prediction of additively manufactured material: Effects of heat treatment and build orientation," *Fatigue Fract. Eng. Mater. Struct.*, vol. 43, no. 4, pp. 831–844, 2020, doi: 10.1111/ffe.13200.
[35] D. L. McDowell and F. P. Dunne, "Microstructure-sensitive computational modeling of fatigue crack formation," *Int. J. Fatigue*, vol. 32, no. 9, pp. 1521–1542, 2010, doi: 10.1016/j.ijfatigue.2010.01.003.